Journal of the European Ceramic Society xxx (2016) xxx–xxx

Contents lists available at www.sciencedirect.com

Journal of the European Ceramic Society

journal homepage: www.elsevier.com/locate/jeurceramsoc

Structural, thermal and dielectric properties of rare earth substituted eulytite for LTCC applications

Pullanchiyodan Abhilash[a,b], Mailadil Thomas Sebastian[c], Kuzhichalil Peethambharan Surendran[a,b,*]

[a] Materials Science and Technology Division, National Institute for Interdisciplinary Science and Technology (NIIST- CSIR), Thiruvananthapuram 695019, India
[b] Academy of Science and Innovative Research (AcSIR), India
[c] Microelectronics and Materials Physics Laboratories, University of Oulu, PO BOX 4500, FIN-90014 Oulu, Finland

ARTICLE INFO

Article history:
Received 13 October 2015
Received in revised form 26 January 2016
Accepted 7 February 2016
Available online xxx

Keywords:
Crystal structure
LTCC
Microwave ceramics
Sintering
Rare earth

ABSTRACT

A new series of LTCC compositions having the general formula $Bi_{3.9}RE_{0.1}(SiO_4)_3$ where, (RE = Yb, Tm, Er, Gd, Sm, Nd, Pr) were developed. The crystal structure analysis using Rietveld refinement of the powder diffraction data of all compositions confirmed partial substitution of rare earth at bismuth site. The microwave dielectric and thermal properties of these new LTCC compositions were studied. Some of the rare earth substituted compound namely, $Bi_{3.9}Tm_{0.1}(SiO_4)_3$, $Bi_{3.9}Sm_{0.1}(SiO_4)_3$, show improvement in $Q_u \times f$ value (22,600 GHz and 24,100 GHz respectively at 8.2 GHz) as compared to the parent $Bi_4(SiO_4)_3$ (20,500 GHz, at 8.2 GHz).

1. Introduction

With the advent of 'mobile phone revolution', the miniaturization of the microwave devices is one of the major challenges in electronic industry. Due to their low-manufacturing cost, excellent performance, and high level of integration the low temperature co-fired ceramic (LTCC) technology has emerged as a crucial step towards the fabrication of 3D integrated circuits [1–7]. In typical LTCC techniques, highly conducting silver (Ag) metal is commonly used as the electrode material, despite its high cost constraints [8]. The approach of multilayer fabrication helps to integrate the passive components like resistors, capacitors and insulators within individual layers, that helps to reduce the size and cost of the multi-chip module [9,10]. The LTCC technology get a wide variety of application including microsystem, multilayer capacitors, sensors and actuators, chip antennas, Filters, automobiles, RF applications, aerospace, SOFC components etc. [11–15]. The primary requirements of an LTCC material are low dielectric constant, low dielectric loss or high quality factor, high thermal conductivity, low coefficient of thermal expansion, temperature stability of dielectric properties and most importantly the sintering temperature should be less than the melting point of silver (961 °C) [16–20]. Apart from developing novel materials and methods, considerable efforts have been made, in establishing structure-property correlation of the reported dielectric materials [1]. Furthermore, several reports were recently published describing the effect of various dopants including rare earth ions on the physical properties of the ceramic solid solutions [21–25].

Among several of dielectric materials developed, bismuth silicate, $[Bi_4(SiO_4)_3$, BSO] has received a resurged interest by the ceramic industries due to its multifunctionality possessing interesting dielectric, thermoluminescent and photocatalytic characteristics. The crystal structure features of $Bi_4(SiO_4)_3$ were elucidated by Liu and Kuo in 1997 [26]. Of late in 2014, Xiong et al. reported the UV excited fluorescence and thermoluminescence spectra of pure and rare-earth-doped bismuth silicate crystals grown by the modified Bridgman method [27]. Batool et al. recently investigated the photocatalytic activity of bismuth modified silica nano fibres (based on $Bi_4(SiO_4)_3$) and reported enhancement in photocatalytic activity as compared with pure silica [28]. As hinted before, the bismuth silicate is also an interesting dielectric material as well. Though Sirdeshmukh and Reddy in 1980 reported

* Corresponding author at: Materials Science and Technology Division, National Institute for Interdisciplinary Science and Technology (NIIST- CSIR), Thiruvananthapuram 695019, India. Fax: +91 471 2491712.
E-mail addresses: kpsurendran@niist.res.in, drkpsurendran@yahoo.com (K.P. Surendran).

http://dx.doi.org/10.1016/j.jeurceramsoc.2016.02.019
0955-2219/

the dielectric properties of $Bi_4(SiO_4)_3$ single crystal [29], their microwave dielectric properties were largely unknown until 2008 when Kim et al. [30,31] suggested it as a suitable material for LTCC substrate for microelectronic applications. More recently, Abhilash et al. developed glass-free $Bi_4(SiO_4)_3$ LTCC tapes [2] with excellent microwave dielectric properties. With an objective of improving the dielectric properties, in the present paper, we explore the effect of rare earth substitution on the structural and dielectric properties of $Bi_{3.9}RE_{0.1}(SiO_4)_3$, (RE = Yb, Tm, Er, Gd, Sm, Nd, Pr) ceramics.

2. Experimental

2.1. Methodology

The $Bi_{3.9}RE_{0.1}(SiO_4)_3$ (BRESO) ceramic were prepared through conventional solid state ceramic route. The required amount of the precursors, Bi_2O_3 (<10 μm, 99.9%, Sigma–Aldrich, St. Louis, MO, USA) and SiO_2 (325 mesh, 99.6% metal basis, Sigma–Aldrich) and rare earth oxides: Yb_2O_3, Tm_2O_3, Er_2O_3, Gd_2O_3, Sm_2O_3, Nd_2O_3 and Pr_6O_{11} (IRE, Kerala, India) were weighed accurately and mixed in an agate mortar. The resultant mixture was dried overnight at 70 °C in a hot air oven. The dried powder was calcined at 850 °C for 4 h and was subsequently ground into fine powder by ball milling for 48 h using yttria stabilized zirconia balls and ethanol as the grinding media. The ground powder was mixed with 5 wt.% polyvinyl alcohol solution (PVA, molecular weight 22,000, BDH Poole, U.K.), dried and pressed into cylindrical pellets of different dimensions for different property measurements such as microwave dielectric, coefficient of linear thermal expansion and thermal conductivity using uniaxial hydraulic press by applying a pressure of 100 MPa. The pellets were then sintered at 900 °C for 8–12 h in air.

2.2. Characterizations

The phase formation of the calcined powder was identified by X-ray diffraction analysis (PANalytical X'Pert PRO diffractometer having Nickel filtered Cu Kα, Netherlands). Detailed structural investigation of the samples was carried out by Rietveld refinement using commercial X'Pert High Score Plus software. The crystal structure of the BRESO was interpreted using Crystal Maker software. The thermal conductivity (TC) of the sintered ceramic pellets was measured using laser flash thermal property analyzer (Flash Line 2000, Anter Corporation, Pittsburgh, USA). The coefficient of thermal expansion (CTE) was measured using thermomechanical analyzer (TMA/SS7300, SII Nano Technology Inc.). The bulk density of sintered samples was estimated using Archimedes method. The SEM analysis of samples was done using a scanning electron microscope (JEOL JSM 5600LV, Tokyo, Japan). For SEM analysis, the surface of sintered samples was mirror polished and then thermally etched below 20 °C of the sintering temperature at very fast heating and cooling rates. The microwave dielectric properties were measured using a vector network analyzer (Model No. E5071C ENA series; Agilent Technologies, Santa Clara, CA). The relative permittivity (ε_r) of the samples was measured by the Hakki–Coleman method modified by Courtney [32] in the frequency range of 8–12 GHz. The unloaded quality factor was measured by the resonant cavity method [32].The temperature variation of resonant frequency (τ_f) and temperature variation of dielectric constant (τ_ε) of the samples were measured in the temperature range of 25 °C–70 °C in Hakki–Coleman method [32].

3. Results and discussions

In order to examine the solid solubility of rare earth at the bismuth site, we have chosen Sm^{3+} as the typical rare earth cation

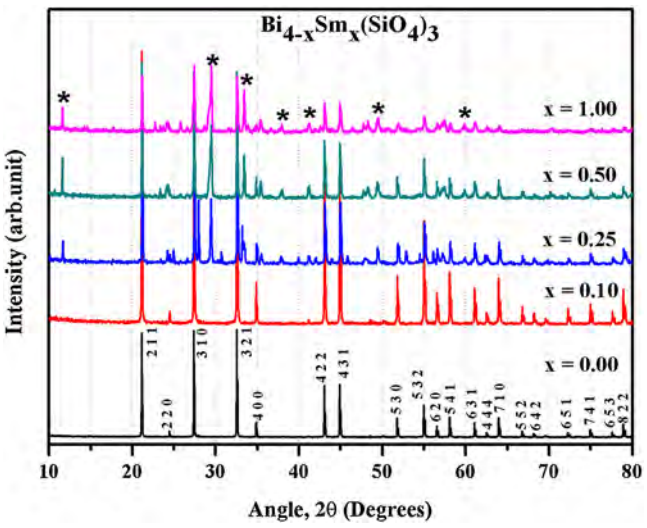

Fig. 1. XRD patterns of $Bi_{4-x}Sm_x(SiO_4)_3$ calcined at 850 °C for 4 h (the secondary phase of Sm_2O_3 is represented by asterisk).

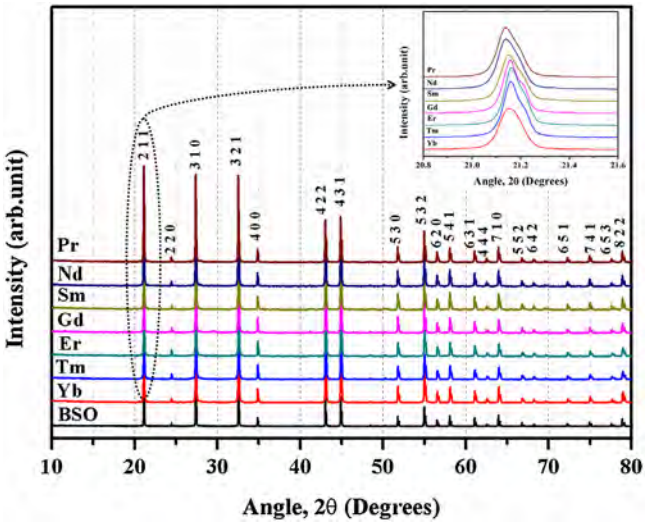

Fig. 2. XRD patterns of BSO and BRESO (RE = Yb, Tm, Er, Gd, Sm, Nd, and Pr) calcined at 850 °C for 4 h. The inset shows the magnified image of [2 1 1] peak.

to be substituted for Bi^{3+} due to their similarity in ionic radius. A series of samarium substituted samples having a general formula $Bi_{4-x}Sm_x(SiO_4)_3$ were prepared, [x = 0.00, 0.10, 0.25, 0.50 and 1.00 respectively]. The XRD patterns of the $Bi_{4-x}Sm_x(SiO_4)_3$ powders calcined at 850 °C for 4 h are shown in Fig. 1.

From the Figure, one could clearly observe that for compositions up to x = 0.10 only form a solid solution, where all the relevant peaks in this XRD pattern can be well indexed using standard JCPDS file of parent bismuth silicate (JCPDS file 35–1007) having cubic structure with $I\bar{4}3d$ space group. As the substitution concentration increases from 0.10, additional peaks could be observed in the XRD patterns (represented by asterisk) which correspond to Sm_2O_3. Hence, the optimum rare earth ion concentration to form complete solid solution was restricted up to x = 0.10, and all other rare earth substitution in bismuth silicate used in this study was carried out with x = 0.10 only.

Fig. 2 represents the XRD patterns of pure BSO and BRESO powder calcined at 850 °C for 4 h. It is evident from the Figure that all the rare earth substituted compound form complete solid solution, and all peaks in the XRD pattern could be indexed using standard JCPDS file (JCPDS file 35–1007). The inset of the Figure shows the

Please cite this article in press as: P. Abhilash, et al., Structural, thermal and dielectric properties of rare earth substituted eulytite for LTCC applications, *J Eur Ceram Soc* (2016), http://dx.doi.org/10.1016/j.jeurceramsoc.2016.02.019

Table 1
Rietveld refinement data of BRESO.

Material	Lattice constant (Å)	R_{exp}(%)	R_p(%)	R_{wp} (%)	χ^2
$Bi_{3.9}Yb_{0.1}(SiO_4)_3$	10.2776(2)	16.00	17.02	19.66	1.51
$Bi_{3.9}Tm_{0.1}(SiO_4)_3$	10.2788(2)	10.58	11.82	14.61	1.91
$Bi_{3.9}Er_{0.1}(SiO_4)_3$	10.2790(2)	16.65	15.71	18.48	1.23
$Bi_{3.9}Gd_{0.1}(SiO_4)_3$	10.2833(1)	16.17	13.54	16.84	1.08
$Bi_{3.9}Sm_{0.1}(SiO_4)_3$	10.2837(1)	15.32	15.16	18.69	1.49
$Bi_{3.9}Nd_{0.1}(SiO_4)_3$	10.2843(1)	10.17	10.59	13.66	1.80
$Bi_{3.9}Pr_{0.1}(SiO_4)_3$	10.2851(1)	10.36	10.53	13.79	1.77

enlarged portion of the peaks around 2θ angle 21.15°. Interestingly, one can clearly observe a slight shift in this peak's position towards lower angle as the RE ionic radii increases from Yb to Pr. This shift is believed to be due to the expansion of unit cell lattice resulting from the increase in ionic size of partially substituted rare earth ions from Yb to Pr. This result indicates that all the RE ions considered in this investigation partially substitute for Bi to form a solid solution up to a limiting value of about $x = 0.10$. The solid solubility of other RE ions may be slightly different but expected to be close to that of Sm.

In order to understand the structural modification resulting from the partial substitution, a more detailed powder diffraction analysis was carried out by Rietveld refinement using X-pert high score plus software. The quality of the fitting between the experimental and calculated profile is assessed by the various R parameters like R_p (profile factor), R_{wp} (weighted profile factor), R_{exp} (expected weight profile factor) and the goodness of fit (GOF, χ^2) described below [33].

$$R_p = 100\frac{\sum_{i=1}^{n}|y_i - y_{c,i}|}{\sum_{i=1}^{n} y_i}$$

Where 'y_i', '$y_{c,i}$' and 'n' indicates the experimental, calculated and total number of points respectively.

$$R_{wp} = 100\left[\frac{\sum_{i=1}^{n}\omega_i|y_i - y_{c,i}|^2}{\sum_{i=1}^{n}\omega_i y_i^2}\right]^{\frac{1}{2}}$$

Here the 'ω_i' is the reciprocal of the variance of observation y_i.

$$R_{exp} = 100\left[\frac{n-p}{\sum_{i=1}^{n}\omega_i y_i^2}\right]^{\frac{1}{2}}$$

Here $(n-p)$ is represents the number of degrees of freedom ('n' is the total number of experimental points and 'p' is the number of refined parameters).

$$X^2 = \left[\frac{R_{wp}}{R_{exp}}\right]^2$$

Table 1 represents the best-fitted refinement data of all the rare earth substituted samples. Evidently, the lattice constant shows a gradual increase with increase in the ionic radii of rare earth. The GOF (goodness of fit, χ^2) value of all the material comes less than 2, which indicate best fit of calculated and observed XRD patterns, within the limits of experimental error. The refinement parameter of $Bi_{3.9}Nd_{0.1}(SiO_4)_3$ (R_p(%) = 10.59, R_{exp}(%) = 10.17, R_{wp}(%) = 13.66 and χ^2 = 1.80) shows better results.

Fig. 3 (a) represents a typical Rietveld refined powder diffraction spectrum of Nd substituted BRESO including observed, calculated and difference plot. Based on the refinement data, the crystal structure of BRESO was elucidated using *Crystal Maker* software.

Fig. 3 (b and c) show the crystal structure of $Bi_{3.9}Nd_{0.1}(SiO_4)_3$ as a representative for BRESO. Fig. 3(b) represents the ball and stick model while 3(c) is the polyhedron. As reported, eulytite structure can be represented as a three-dimensional packing of $(SiO_4)^{4-}$

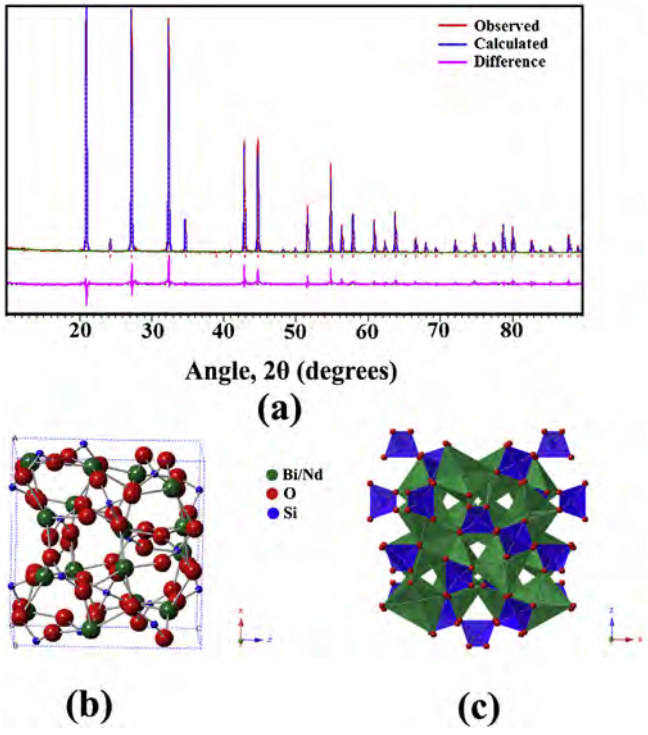

Fig. 3. (a): Rietveld refinement spectrum of $Bi_{3.9}Nd_{0.1}(SiO_4)_3$ (b) and (c) are the crystal structure of $Bi_{3.9}Nd_{0.1}(SiO_4)_3$ in ball and stick model and polyhedron respectively.

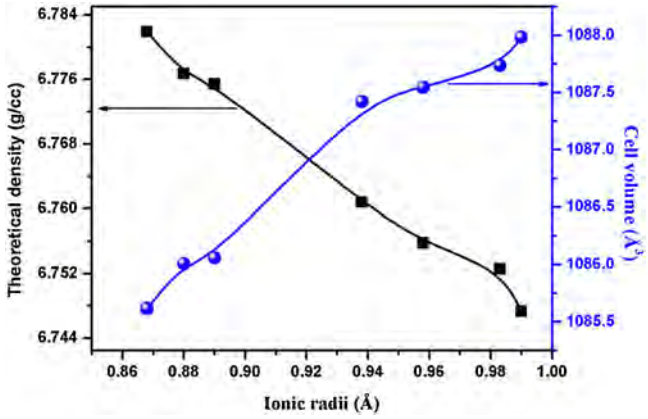

Fig. 4. Variation of cell volume and density with RE ionic.

tetrahedral and $(BiO_6)^{9-}$ octahedron with common sharing edges [34,35]. The Si—O bond length is about 1.612 Å, which is in agreement with bond length commonly found in orthosilicates [36]. The Bi/Nd—O bond shows two types bond lengths, three shorter bond length of 2.180 Å and three longer bond length of 2.589 Å to form a distorted octahedron. It is believed that the distortion is due to the presence of $6s^2$ electron in outer orbital of bismuth ion [26]. The O—Si—O angles in the $(SiO_4)^{4-}$ tetrahedron shows two different kinds of bond angles like 114.23° and 107.15° respectively. The different bond angles reveal that the tetrahedron is a distorted one which is in agreement with the earlier report [26].

Fig. 4 represents the variation of cell volume and density with respect to ionic radii of the substituted rare earth ion. The cell volume shows a linear increase with ionic radii of rare earth whereas the density shows a converse trend as expected. This is because the substitution of a bigger sized rare earth ion result in the expansion of the unit cell that in turn causing a decrease in density as a function of the ionic radius of the rare earth. This result serves as an

Please cite this article in press as: P. Abhilash, et al., Structural, thermal and dielectric properties of rare earth substituted eulytite for LTCC applications, *J Eur Ceram Soc* (2016), http://dx.doi.org/10.1016/j.jeurceramsoc.2016.02.019

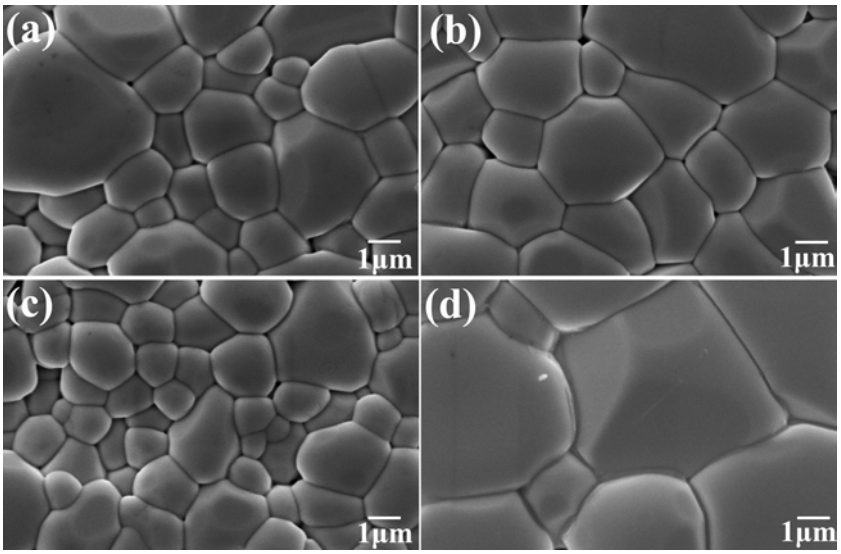

Fig. 5. SEM images of polished and thermally etched surfaces of (a) $Bi_{3.9}Er_{0.1}(SiO_4)_3$ (b) $Bi_{3.9}Sm_{0.1}(SiO_4)_3$ (c) $Bi_{3.9}Yb_{0.1}(SiO_4)_3$ and (d) $Bi_{3.9}Nd_{0.1}(SiO_4)_3$ (sintered at 900 °C–8 h).

additional proof for a partial solid solution formation of rare earth at the bismuth site based on $Bi_{3.9}RE_{0.1}(SiO_4)_3$.

The surface SEM images of the rare earth substituted bismuth silicate solid solution were recorded from sintered samples after mirror polishing and thermal etching. Fig. 5 represents the SEM images of polished and thermally etched surfaces of (a) $Bi_{3.9}Er_{0.1}(SiO_4)_3$ (b) $Bi_{3.9}Sm_{0.1}(SiO_4)_3$ (c) $Bi_{3.9}Yb_{0.1}(SiO_4)_3$ and (d) $Bi_{3.9}Nd_{0.1}(SiO_4)_3$ as representatives. The SEM images clearly show good densification and devoid of any additional phases. Except for $Bi_{3.9}Nd_{0.1}(SiO_4)_3$, all other materials have almost similar grain size, whereas the Nd substituted compound has a relatively higher grain size.

The microwave dielectric properties of the BRESO and parent BSO are given in Table 2 along with their sintering conditions. All the rare earth substituted samples have the same sintering temperature as that of parent BSO (900 °C for 8 h). However compositions such as $Bi_{3.9}Gd_{0.1}(SiO_4)_3$ and $Bi_{3.9}Pr_{0.1}(SiO_4)_3$ showed a higher sintering duration (12 h), as compared to other rare earth doped specimen studied in the present investigation. Evidently, the sintered materials show good densification above 90% for all the compositions. The porosity corrected ε_r of the BRESO is calculated using the equation of Penn et al. [37] and are also given in the Table. The ε_r of the samples vary from 15.5 to 16.3. The $Q_u \times f$ values of some of the rare earth substituted sample ($Bi_{3.9}Tm_{0.1}(SiO_4)_3$, $Bi_{3.9}Sm_{0.1}(SiO_4)_3$) show improvement as compared to the parent BSO. The τ_f values of the BRESO vary from −84 to −74 ppm/°C. It should be noted that repeated experiment on pure eulytite [$Bi_4(SiO_4)_3$] consistently gave a $Q_u \times f$ of value 20500 GHz (at 8.2 GHz) and τ_f −73 ppm/°C. However, these values are markedly different from an earlier report by Kim et al. [30] who reported a $Q_u \times f$ value of 36101 GHz and τ_f −9.42 ppm/°C. The exact reason for this discrepancy is unknown, but can be attributed to factors such as the origin and purity of the raw materials, synthesizing and measurement conditions. The τ_ε of all these materials were calculated and the results are given in Table 2. It was obvious from Table that the τ_ε value varies within the limit of 147–167 ppm/°C for rare earth substituted ions. The parent BSO shows a little lower value (131 ppm/°C) compared to rare earth substituted ceramics, and this value is only slightly different from the report of Valant et al. (115 ppm/K) [38].

The heat dissipation from the substrate material is one of the major concerns in the electronic industry. In recent years considerable attention has been paid to improve the thermal conductivity of

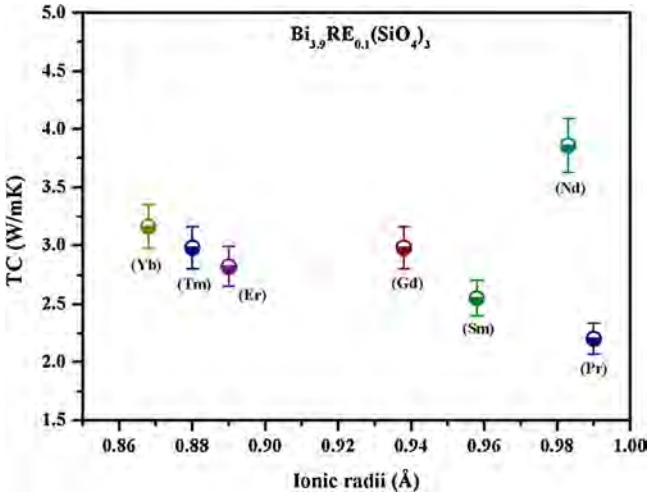

Fig. 6. Room temperature thermal conductivity (TC) of BRESO.

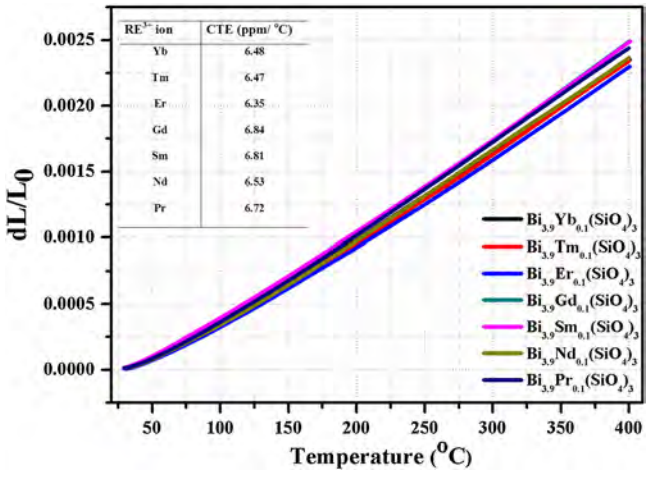

Fig. 7. CTE value of BRESO from room temperature to 400 °C.

LTCC materials. The porosity corrected room temperature thermal conductivity (TC) of BRESO compositions is shown in Fig. 6. The TC value of the BRESO compounds varies from 2.2 to 3.8 W/m K.

Please cite this article in press as: P. Abhilash, et al., Structural, thermal and dielectric properties of rare earth substituted eulytite for LTCC applications, *J Eur Ceram Soc* (2016), http://dx.doi.org/10.1016/j.jeurceramsoc.2016.02.019

Table 2
Microwave dielectric properties of BSO and BRESO.

Material	SinteringTemp. (°C)	Density(%, ±1)	ε_r(Measured,±1%)	ε_r(porosity corrected)	$Q_u \times f$(GHz,±2%)	τ_f(ppm/°C,±2%)	τ_ε(ppm/°C,±2%)
$Bi_4(SiO_4)_3$	900	94	14.5	15.8	20500	−73	131
$Bi_{3.9}Yb_{0.1}(SiO_4)_3$	900	95	14.9	16.0	19000	−84	167
$Bi_{3.9}Tm_{0.1}(SiO_4)_3$	900	93	14.0	15.5	22600	−84	156
$Bi_{3.9}Er_{0.1}(SiO_4)_3$	900	95	14.9	16.0	19500	−74	147
$Bi_{3.9}Gd_{0.1}(SiO_4)_3$	900	91	14.3	16.3	18200	−74	149
$Bi_{3.9}Sm_{0.1}(SiO_4)_3$	900	93	14.4	15.9	24100	−83	164
$Bi_{3.9}Nd_{0.1}(SiO_4)_3$	900	92	14.2	15.9	20000	−82	166
$Bi_{3.9}Pr_{0.1}(SiO_4)_3$	900	92	14.0	15.7	19900	−77	154

Some of the rare earth substituted solid solution shows marginally improved thermal conductivity as compared to the parent BSO (2.82 W/m K.) [2]. The thermal conductivity in general decrease with increase in ionic radii of the rare ions with the exception of Nd and the variation is almost linear. The slightly higher thermal conductivity of Nd substitution (3.8 W/m K) is due to its higher grain size which decreases the grain boundary region [39].

The coefficient of linear thermal expansion (CTE or α_L) is also a major criterion for the practical application of an LTCC substrate. Fig. 7 shows the variation of CTE values of BRESO from room temperature to 400 °C. The average CTE value of all the rare earth substituted compositions were shown in the inset of the Figure. From the Figure it is clear that all the materials show a linear variation with temperature, and the average CTE value of all the rare earth doped compositions are between 6.35 to 6.84 ppm/°C, while it is marginally lower than the parent BSO (7.09 ppm/°C) [2].

4. Conclusions

The effect of rare earth doping (RE = Yb, Tm, Er, Gd, Sm, Nd, Pr) on the physical, thermal and dielectric properties of $Bi_4(SiO_4)_3$ (eulytite) was investigated. $Bi_{3.9}RE_{0.1}(SiO_4)_3$ compositions were prepared through conventional solid state synthesis. The sintering temperature of all the composition was optimized for its maximum densification and was 900 °C. The room temperature thermal conductivity of all the rare earth substituted samples were measured, where $Bi_{3.9}Nd_{0.1}(SiO_4)_3$ gave the maximum thermal conductivity of 3.8 W/m.K. The average CTE of all the samples in the temperature range of 30 to 400 °C were measured and the result indicates that the values vary from 6.35 to 6.84 ppm/°C, which are lower than the parent material BSO (7.09 ppm/°C). The detailed crystal structure studies using Rietveld refinement of the powder XRD showed that all the composition form solid solution only up to about 10 mol % of the substituent. The microwave dielectric properties show that the $Bi_{3.9}Sm_{0.1}(SiO_4)_3$ gives the best $Q_u \times f$ value which is around 24,100 GHz (at 8.2 GHz).

Acknowledgements

The authors acknowledge Council of Scientific and Industrial Research, New Delhi and Department of Science and Technology for financial assistance. The authors are thankful to Ms. Soumya and Dr. P. Prabhakar Rao for SEM analysis.

References

[1] D. Zhou, W.-B. Li, H.-H. Xi, L.-X. Pang, G.-S. Pang, Phase composition, crystal structure, infrared reflectivity and microwave dielectric properties of temperature stable composite ceramics (scheelite and zircon-type) in $BiVO_4$–YVO_4 system, J. Mater. Chem. C 3 (2015) 2582–2588, http://dx.doi.org/10.1039/C4TC02728K.
[2] P. Abhilash, M.T. Sebastian, K.P. Surendran, Glass free, non-aqueous LTCC tapes of $Bi_4(SiO_4)_3$ with high solid loading, J. Eur. Ceram. Soc. 35 (2015) 2313–2320, http://dx.doi.org/10.1016/j.jeurceramsoc.2015.02.002.
[3] S. Rajesh, H. Jantunen, M. Letz, S. Pichler-Willhelm, Low temperature sintering and dielectric properties of alumina-filled glass composites for LTCC applications, Int. J. Appl. Ceram. Technol. 9 (2012) 52–59, http://dx.doi.org/10.1111/j.1744-7402.2011.02684.x.
[4] M. Valant, D. Suvorov, processing and dielectric properties of sillenite compounds Bi_{12} $MO_{20-\delta}$ (M = Si, Ge, Ti, Pb, Mn, $B_{1/2}P_{1/2}$), J. Am. Ceram. Soc. 84 (2001) 2900–2904, http://dx.doi.org/10.1111/j. 1151-2916.2001. tb01112. x.
[5] S.D. Rama Rao, S. Roopas Kiran, V.R.K. Murthy, Correlation between structural characteristics and microwave dielectric properties of scheelite $Ca_{1-x}Cd_xMoO_4$ solid solution, J. Am. Ceram. Soc. 95 (2012) 3532–3537, http://dx.doi.org/10.1111/j.1551-2916.2012.05317.x.
[6] W. Huang, K.-S. Liu, L.-W. Chu, G.-H. Hsiue, I.-N. Lin, Microwave dielectric properties of LTCC materials consisting of glass–$Ba_2Ti_9O_{20}$ composites, J. Eur. Ceram. Soc. 23 (2003) 2559–2563, http://dx.doi.org/10.1016/S0955-2219(03) 00172-9.
[7] C.-Y. Liu, B.-G. Tsai, M.-H. Weng, S.-J. Huang, Influence of B_2O_3 additive on microwave dielectric properties of $Li_2ZnTi_3O_8$ ceramics for LTCC applications, Int. J. Appl. Ceram. Technol. 10 (2013) E49–56, http://dx.doi.org/10.1111/j.1744-7402.2012.02835.x.
[8] E.K. Suresh, A.N. Unnimaya, A. Surjith, R. Ratheesh, New vanadium based $Ba_3MV_4O_{15}$ (M = Ti and Zr) high Q ceramics for LTCC applications, Ceram. Int. 39 (2013) 3635–3639, http://dx.doi.org/10.1016/j.ceramint.2012.10.192.
[9] A. Bittner, H. Seidel, U. Schmid, High-frequency characterization of porous low-temperature cofired ceramics substrates, J. Am. Ceram. Soc. 93 (2010) 3778–3781, http://dx.doi.org/10.1111/j.1551-2916.2010.03928.x.
[10] M.T. Sebastian, H. Jantunen, Low loss dielectric materials for LTCC applications: a review, Int. Mater. Rev. 53 (2008) 57–90, http://dx.doi.org/10.1179/174328008x277524.
[11] T. Thelemann, H. Thust, M. Hintz, Using LTCC for microsystems, Microelectron. Int. 19 (2002) 19–23, http://dx.doi.org/10.1108/13565360210445005.
[12] T. Maeder, C. Slater, B. Jiang, F. Vecchio, C. Jacq, P. Ryser, 3D structuration of LTCC and related technologies for thermal management and microfluidic structures, J. Microelectron. Electron Components Mater. 42 (2012) 234–244.
[13] J. Varghese, S. Gopinath, M.T. Sebastian, Effect of glass fillers in $Cu_2ZnNb_2O_8$ ceramics for advanced microwave applications, Mater. Chem. Phys. 137 (2013) 811–815, http://dx.doi.org/10.1016/j.matchemphys.2012.10.014.
[14] L.J. Golonka, Technology and applications of low temperature cofired ceramic (LTCC) based sensors and microsystems, Bull. POLISH Acad. Sci. Tech. Sci. 54 (2006) 221–231.
[15] D. Jurków, T. Maeder, A. Dąbrowski, M.S. Zarnik, D. Belavič, H. Bartsch, et al., Overview on low temperature co-fired ceramic sensors, Sens. Actuators A Phys. 233 (2015) 125–146, http://dx.doi.org/10.1016/j.sna.2015.05.023.
[16] S. George, P.S. Anjana, V.N. Deepu, P. Mohanan, M.T. Sebastian, Low-temperature sintering and microwave dielectric properties of Li_2MgSiO_4 ceramics, J. Am. Ceram. Soc. 92 (2009) 1244–1249, http://dx.doi.org/10.1111/j.1551-2916.2009.02998.x.
[17] S. George, M.T. Sebastian, Low-temperature sintering and microwave dielectric properties of $Li_2ATi_3O_8$ (A = Mg, Zn) ceramics, Int. J. Appl. Ceram. Technol. 8 (2011) 1400–1407, http://dx.doi.org/10.1111/j.1744-7402.2010.02590.x.
[18] D. Thomas, P. Abhilash, M.T. Sebastian, Casting and characterization of $LiMgPO_4$ glass free LTCC tape for microwave applications, J. Eur. Ceram. Soc. 33 (2013) 87–93, http://dx.doi.org/10.1016/j.jeurceramsoc.2012.08.002.
[19] D. Thomas, M.T. Sebastian, Effect of Zn^{2+} substitution on the microwave dielectric properties of $LiMgPO_4$ and the development of a new temperature stable glass free LTCC, J. Eur. Ceram. Soc. 32 (2012) 2359–2364, http://dx.doi.org/10.1016/j.jeurceramsoc.2012.01.031.
[20] R.C. Pullar, C. Lai, F. Azough, R. Freer, N.M. Alford, Novel microwave dielectric LTCCs based upon V_2O_5 doped $M^{2+}Cu_2Nb_2O_8$ compounds (M^{2+} = Zn, Co, Ni, Mg and Ca), J. Eur. Ceram. Soc. 26 (2006) 1943–1946, http://dx.doi.org/10.1016/j.jeurceramsoc.2005.09.083.
[21] T. Groń, E. Tomaszewicz, Z. Kukuła, S. Pawlus, B. Sawicki, Dielectric permittivity of some novel copper/cobalt and rare-earth metal tungstates, Mater. Sci. Eng. B 184 (2014) 14–17, http://dx.doi.org/10.1016/j.mseb.2014.01.006.
[22] K. Mori, H. Ogawa, A. Kan, H. Ohsato, S. Ishihara, Crystal structural characterization of Nd_2BaZnO_5-type microwave dielectric ceramics with rare-earth substitutions for Nd, Mater. Chem. Phys. 79 (2003) 273–275, http://dx.doi.org/10.1016/S0254-0584(02) 00275-4.
[23] Y.-X. Li, X. Yao, X.-S. Wang, Y.-B. Hao, Studies of dielectric properties of rare earth (Dy, Tb, Eu) doped barium titanate sintered in pure nitrogen, Ceram. Int. 38 (2012) S29–32, http://dx.doi.org/10.1016/j.ceramint.2011.04.042.

Please cite this article in press as: P. Abhilash, et al., Structural, thermal and dielectric properties of rare earth substituted eulytite for LTCC applications, *J Eur Ceram Soc* (2016), http://dx.doi.org/10.1016/j.jeurceramsoc.2016.02.019

[24] K.M. Manu, C. Karthik, L.-C. Leu, K.A. Lazar, R. Ubic, M.T. Sebastian, crystal structure and microwave dielectric properties of $LiRE_9(SiO_4)_6O_2$ Ceramics (RE = La,Pr,Nd,Sm,E. Gd, and Er), J. Am. Ceram. Soc. 96 (2013) 1504–1511, http://dx.doi.org/10.1111/jace.12215.
[25] D.C. Kakarla, K.M. Jyothinagaram, A.K. Das, V. Adyam, Dielectric and magnetodielectric properties of R_2NiMnO_6 (R=Nd, Eu, G. Dy, and Y), J. Am. Ceram. Soc. 9 (2014) 1–9, http://dx.doi.org/10.1111/jace.13039.
[26] L.I.U. Hongchao, K.U.O. Changlin, X-ray powder diffraction pattern of $Bi_4(SiO_4)_3$, J. Mater. Sci. Technol. 13 (1997) 145–148.
[27] Z. Xiong, J. Xu, Y. Zhang, Z. Tan, H. Shen, B. Yang, et al., Emission spectra and thermoluminescence of rare-earth-doped bismuth silicate crystals grown by modified Bridgman method, J. Cryst. Growth 401 (2014) 305–307, http://dx.doi.org/10.1016/j.jcrysgro.2014.01.024.
[28] S.S. Batool, S. Hassan, Z. Imran, M a. Rafiq, M. Ahmad, K. Rasool, et al., The enhancement in photocatalytic activity of bismuth modified silica and bismuth silicate nanofibers, Catal. Commun. 49 (2014) 39–42, http://dx.doi.org/10.1016/j.catcom.2014.02.001.
[29] L. Sirdeshmukh, Y.R. Reddy, Dielectric properties of $Bi_4(GeO_4)_3$ and $Bi_4(SiO_4)_3$, Bull. Mater. Sci. 2 (1980) 61–66, http://dx.doi.org/10.1007/BF02748536.
[30] J.-S. Kim, M.-R. Joung, M.-E. Song, S. Nahm, J.-H. Paik, B.-H. Choi, et al., Synthesis and microwave dielectric properties of $Bi_4(SiO_4)_3$ ceramics, J. Am. Ceram. Soc. 91 (2008) 3461–3464, http://dx.doi.org/10.1111/j.1551-2916.2008.02657.x.
[31] M.-R. Joung, J.-S. Kim, M.-E. Song, D.-S. Paik, S. Nahm, J.-H. Paik, et al., Effect of B_2O_3 on the sintering condition and microwave dielectric properties of $Bi_4(SiO_4)_3$ ceramics, J. Am. Ceram. Soc. 91 (2008) 4165–4167, http://dx.doi.org/10.1111/j.1551-2916.2008.02819.x.
[32] M.T. Sebastian, Dielectric Materials for Wireless communication, 1st, Elsevier, Amsterdam, 2008, pp. 16–23.
[33] V. Kumar, S. Kumari, P. Kumar, M. Kar, L. Kumar, Structural analysis by rietveld method and its correlation with optical propertis of nanocrystalline zinc oxide, Adv. Mater. Lett. 6 (2015) 139–147, http://dx.doi.org/10.5185/amlett.2015.5632.
[34] E.H. Arbib, B. Elouadi, J.P. Chaminade, J. Darriest, The crystal structure of the phosphate eulytite $Ba_3Bi(PO_4)_3$, Mater. Res. Bull. 35 (2000) 761–773.
[35] P.P. Sahoo, T.N. Guru Row, Crystal chemistry of the noncentrosymmetric eulytites: $A_3Bi(XO_4)_3$ (X = V, A = Pb; X = P, A=Ca, Cd, Sr, Pb), Inorg. Chem. 49 (2010) 10013–10021, http://dx.doi.org/10.1021/ic101316u.
[36] D.J. Segal, R.P. Santoro, R.E. Newnham, Neutron-diffraction study of $Bi_4Si_3O_{12}$, Zeitschrift Für Krist 123 (1966) 73–76.
[37] S.J. Penn, N.M. Alford, A. Templeton, X. Wang, M. Xu, M. Reece, et al., Effect of porosity and grain size on the microwave dielectric properties of sintered alumina, J. Am. Ceram. Soc. 80 (1997) 1885–1888, http://dx.doi.org/10.1111/j.1151-2916.1997.tb03066.x.
[38] M. Valant, D. Suvorov, New generation of LTCC materials, Bol. Soc. Esp. Ceram. V 43 (2004) 634–639.
[39] M. Kitayama, K. Hirao, K. Watari, M. Toriyama, S. Kanzaki, Thermal conductivity of β-Si_3N_4: III, effect of rare-earth (RE = La, Nd, Gd, Y, Yb, and Sc) oxide additives, J. Am. Ceram. Soc. 84 (2001) 353–358, http://dx.doi.org/10.1111/j.1151-2916.2001.tb00662.x.

Please cite this article in press as: P. Abhilash, et al., Structural, thermal and dielectric properties of rare earth substituted eulytite for LTCC applications, *J Eur Ceram Soc* (2016), http://dx.doi.org/10.1016/j.jeurceramsoc.2016.02.019